Synthesis and Characterization of WO₃·0.33H₂O/Ag₂MoO₄ Composites as a Visible-Light-Driven Photocatalyst for Rhodamine B and Levofloxacin Degradation

[1]Yun-Xuan Fu, [1]Yan Li, [1]Tian-Long Chang, [1]Xu-Tao Liu, [1]Xiang-Feng Wu, [1,2]Jia-Rui Zhang
[1]Hui Wang* and [1]Xiao-Ye Ma

[1]*School of Materials Science and Engineering, Hebei Key Laboratory of Advanced Materials for Transportation Engineering and Environment, Shijiazhuang Tiedao University, Shijiazhuang 050043, China.*
[2]*Tianjin Key Laboratory of Building Green Functional Materials, Tianjin Chengjian University, Tianjin 300384, China.*
[§]YUN-XUAN FU and YAN LI contributed equally to this work and share the first authorship.
hui-wang@stdu.edu.cn*

Summary: Visible-light-driven WO₃·0.33H₂O/Ag₂MoO₄ composites have been prepared by using an *in-situ* growth of Ag₂MoO₄ nanoparticles on the surfaces of WO₃·0.33H₂O. The photocatalytic activities of the samples were studied by degradation of rhodamine B and levofloxacin dilute solution. The synergistic photocatalytic mechanism was also analyzed. Experimental results reveal that the as-developed hybrids have higher photocatalytic activity than pure samples. When the theoretical molar ratio of WO₃·0.33H₂O to Na₂MoO₄·2H₂O is 1:0.15, the as-developed hybrids have the highest photocatalytic degradation efficiency of 99.0% for rhodamine B in 45 min and 40.9% for levofloxacin in 120 min. Furthermore, there are chemical bonds between WO₃·0.33H₂O and Ag₂MoO₄. In addition, the super oxide radicals play the leading role during the photocatalytic degradation process of the samples. This work will provide reference for treatment of organic dyes and antibiotics pollution in water with using solar energy.

Keywords: Semiconductors; Photocatalysis; WO₃·0.33H₂O; Ag₂MoO₄; Composites.

Introduction

In the past decades, organic dyes and antibiotics contaminants in water have attracted great concerns because they can persistently deteriorate human health [1]. In order to deal with this problem, physical adsorption is often used [2]. However, it can not mineralize pollutants, which may reoccur due to their desorption during the environmental changes. Therefore, it is very necessary to develop a new treatment way of green, efficient and non-secondary pollution. In fact, recently, many Advanced Oxidation Processes (AOPs) have been developed for removal of contaminants from wastewater. Among AOPs, semiconductor photocatalysis, which can easily be driven by the inexhaustible and sustainable sunlight, is deemed as one the most promising technologies to deal with organic dyes and antibiotics [3-8].

For semiconductors, silver molybdate (Ag₂MoO₄), one of high-output molybdates, has been focused because of its unique structure [9]. However, it also has some drawbacks as the same as other noble metal semiconductors, such as costly. Hence, it is important to improve this disadvantage and further enhance its photocatalytic performance. In fact, some effective methods, such as doping metal ions (Eu³⁺

doped β-Ag₂MoO₄ hybrids [10]) and combining it with other semiconductor to fabricate composites (Ag₂MoO₄/Ag/AgBr/GO composites [11]) have been reported. The second method can usually be used to reduce the cost and increase the photocatalytic performances of photocatalyst.

WO₃·0.33H₂O is low-cost, stable under the light illumination and environmentally friendly [12]. It has a small band gap, a large optical absorption range and excellent macroscopic quantum tunnel effect [13-17]. Moreover, it can be used to fabricate composite photocatalyst with other materials, such as Ag [18], Bi₂WO₆ [19], Ag₂O [20] and C [21]. In addition, its energies of conduction band (E_{CB}) and valence band (E_{VB}) are respectively 0.64 and 3.01 eV [22], which can match well with that of Ag₂MoO₄ (E_{CB} = -0.45 eV, E_{VB} = 2.86 eV) [23].

Therefore, in this work, WO₃·0.33H₂O/Ag₂MoO₄ composites were prepared by using an *in-situ* growth of Ag₂MoO₄ nanoparticles on the surface of WO₃·0.33H₂O. Two organics, including rhodamine B (RhB) and levofloxacin (LVFX), were selected to evaluate the photocatalytic activity of the

---

*To whom all correspondence should be addressed.

as-obtained composite. The results show that this method can improve the photocatalytic performance of the pure samples, and the cooperative photocatalytic mechanism of the hybrids is also analyzed. This work has provided a successful sample for the treatment of organic dyes and antibiotic contamination in water under visible light irradiation.

Experimental

Preparation of the WO₃ 0.33H₂O nanoparticle

For WO$_3$·0.33H$_2$O nanoparticle, it was fabricated according to a previous report [12]. In a typical preparation process: 2 mmoL of sodium tungstate dihydrate (Na$_2$WO$_4$·2H$_2$O) and 0.2 mmoL of ethylenediamine tetraacetic acid (EDTA) were fully mixed with 40 mL deionized water for 30 min at room temperature. The pH value was adjusted to 1.0-1.5 by using HCl aqueous solution (3 M). The mixture was then transferred into a 50 mL Teflon-lined stainless steel autoclave. It was sealed and kept in an electric blast drying oven at 180 °C for 6 h and then naturally cooled to the room temperature. The as-obtained WO$_3$·0.33H$_2$O precipitates were separated by centrifugation, washed by distilled water and absolute ethanol and dried in vacuum at 60 °C for 12 h.

Preparation of the WO₃ 0.33H₂O/Ag₂MoO₄ composites

1 mmoL of the as-developed WO$_3$·0.33H$_2$O and 0.03 mmoL silver nitrate (AgNO$_3$) were fully mixed with 20 mL deionized water for 20 min to form solution A. 0.015 mmoL of sodium molybdate dihydrate (Na$_2$MoO$_4$·2H$_2$O) was fully mixed with 20 mL deionized water for 20 min to form solution B. The solution B was then added into the solution A. And the mixed solution was continually stirred for another 1 h. After it was filtered, the as-obtained WO$_3$·0.33H$_2$O/Ag$_2$MoO$_4$ (1:0.15) composite (named as WA-0.15) were washed for 5 times with employing distilled water and absolute ethanol and then dried in vacuum at 60 °C for 6 h. The other samples with theoretically molar ratios of WO$_3$·0.33H$_2$O to Na$_2$MoO$_4$·2H$_2$O, including 1:0.05 (WA-0.05), 1:0.1 (WA-0.1), 1:0.2 (WA-0.2) and 1:0.25 (WA-0.25), were also prepared with the same route. The pure Ag$_2$MoO$_4$, as a control, was also synthesized via the same route without using any WO$_3$·0.33H$_2$O.

Characterization

The structure of the samples was measured by X-ray diffraction (XRD, D8ADVANCE, Bruker Co.,

Germany). The UV-vis diffuse reflectance spectroscopy of the samples was characterized on a UV/VIS/NIR spectrometer (UV-vis DRS, U-4100, Shimadzu Co., Ltd., Japan). The micro-morphology of the samples was observed by using a field emission scanning electron microscope (FE-SEM) (Hitachi SU8010, Japan). The electrochemical impedance spectroscopy (EIS) measurements of the products were carried out on an electrochemical workstation (CHI660E, Shanghai Chenhua Co., China). The elements and valence states of the samples were analyzed by X-ray photoelectron spectroscopy (XPS, ESCALAB 250Xi, Thermo Fisher Scientific Co., USA).

The photocatalytic activity of the samples was assessed by degradation of RhB and LVFX under the visible light irradiation (λ > 420 nm). A Xenon lamp light source system (CEL-HXF300, Beijing Zhongjiao Jinyuan Technology co. Ltd., China) was adopted during the photocatalytic test. For degradation of RhB, 50 mg the as-developed samples and 100 mL 10 mg/L RhB solution were used. Before the light was opened, the mixture was stirred in darkness for 1.5 h to achieve the equilibrium between adsorption and desorption. During the photocatalytic reaction, 4 mL liquid sample was taken at every other 15 min and the supernatant liquid after centrifugation was tested at 554 nm of the characteristic band on an ultraviolet visible spectrophotometer (N4, INESA Analytical Instrument Co., Ltd., China). For degradation of LVFX, similar process was carried out. The difference was that 4 mL liquid sample was taken at every other 30 min during the test and the characteristic band was selected at 288 nm.

Degradation efficiency of the samples was calculated by using Equation (1) [24]:

$$\eta = {C_t}/{C_0} \tag{1}$$

where C_0 and C_t denote the concentration at the adsorption-desorption equilibrium and the sample time t, respectively.

Kinetics of photocatalytic degradation was determined by using Equation (2) [25]:

$$\ln\left({C_0}/{C_t}\right) = \kappa t \tag{2}$$

where C_0 and C_t denote the concentration at the adsorption-desorption equilibrium and the sample time t, respectively. κ denotes the reaction rate constant.

Results and Discussion

Fig. 1 shows the XRD patterns of the samples. It can be seen in Fig. 1(a) that some diffraction peaks are found at 16.5, 27.1, 31.8, 33.3, 38.6, 42.2, 47.8, 50.9, 55.8, 65.7 and 66.6 °, which can be respectively indexed to (111), (220), (311), (222), (400), (331), (422), (511), (440), (533) and (622) planes of cubic b-Ag_2MoO_4 according to JCPDS card No. 08-0473. Besides, in Fig. 1(g), some diffraction peaks are found at 23.1, 24.2, 27.1, 28.3, 33.8, 36.8, 49.5, 50.3, 55.3 and 58.1 °. They are respectively indexed to (002), (200), (131), (220), (202), (222), (400), (260), (402) and (440) crystal planes of the orthorhombic $WO_3 \cdot 0.33H_2O$ according to JCPDS card No.35-0270. Furthermore, it can be seen in Fig. 1(b)-(f) that with increasing the usage amount of Ag_2MoO_4, its characteristic peaks in the as-developed hybrids are gradually increased, while that of $WO_3 \cdot 0.33H_2O$ are gradually decreased. No other peaks are discovered. This indicates that the samples have high purity.
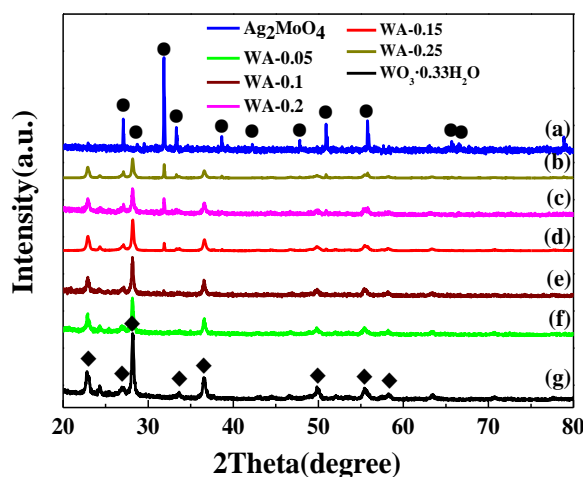

Fig. 1:   XRD spectra of the samples: (a) Ag_2MoO_4, (b)-(f) the as-prepared $WO_3 \cdot 0.33H_2O/Ag_2MoO_4$ with differently theoretical mass ratios of $WO_3 \cdot 0.33H_2O$ to $Na_2MoO_4 \cdot 2H_2O$ and (g) $WO_3 \cdot 0.33H_2O$.

In Fig. 2(a), it shows that the adsorption-desorption equilibrium has been achieved in about 30 min, which is in line with that of Fig. 2(f). Moreover, in Fig. 2(b), with gradually increasing the usage amount of Ag_2MoO_4, the tendency of photocatalytic activity of the samples increases firstly and then declines. When the theoretical molar ratio of $WO_3 \cdot 0.33H_2O$ to $Na_2MoO_4 \cdot 2H_2O$ is 1:0.15, in 45 min, the photocatalytic efficiency of the samples reach the maximum of 99.0%. This is much higher than 0.3% of Ag_2MoO_4 and 1.4% of $WO_3 \cdot 0.33H_2O$. In Fig. 2(c), it shows that all the curves are close to line. This means they are matching with the pseudo-first-order kinetics plot. In Fig. 2(d), the tendency of κ value of the samples is firstly increased and then decreased with increasing the usage amount of Ag_2MoO_4. It is noticed that the as-developed WA-0.15 samples has the highest κ value of 0.0968 min^{-1}, which is 97.7 and 30.3 times as 9.906×10^{-4} of Ag_2MoO_4 and 0.0032 of $WO_3 \cdot 0.33H_2O$, respectively. This result is similar to that of Fig. 2 (b). In Fig. 2 (e), it shows the absorption peak at 554 nm decreases with increasing the degradation time. This phenomenon indicates the destruction of the conjugated structure and RhB may be decomposed into small molecules, e.g., H_2O and CO_2 [24]. In addition, there is a blue shift for the peak from 0 to 60 min. This may be caused by de-ethylation and incomplete mineralization of RhB [26]. In Fig. 2(g), in 120 min, the photocatalytic efficiency is 1.0, 2.9 and 40.9% for Ag_2MoO_4, $WO_3 \cdot 0.33H_2O$ and as-developed WA-0.15 samples, respectively. This means the as-developed composites can not only enhance the photocatalytic degradation activity for RhB but also for LVFX in comparison with pure samples.

In Fig. 3(a), it can be found that Ag_2MoO_4 are irregular nanoparticles with a size rage of 7-9 μm. $WO_3 \cdot 0.33H_2O$ are 2-3 μm spherical particles which are self-assembled by nanosheets. The WA-0.15 samples are 4-5 μm $WO_3 \cdot 0.33H_2O$ spherical particles with coating a layer of Ag_2MoO_4 nanoparticles. This structure makes the hybrids more compacted and is in favor of improving the photocatalytic performances. In addition, W, O, Ag and Mo elements of the as-developed WA-0.15 can be seen in Fig.3 (e)-(h). There is no other impurity, which is consistent with the result of XRD. In Fig. 4 (a), it can be seen that the absorption edge of Ag_2MoO_4 and $WO_3 \cdot 0.33H_2O$ was at about 388 nm and 488 nm. Moreover, that of the as-developed WA-0.15 samples exhibits red-shift, which indicates it possesses wider light response range than pure samples. This is also in line with Fig. 2(b) and (g).
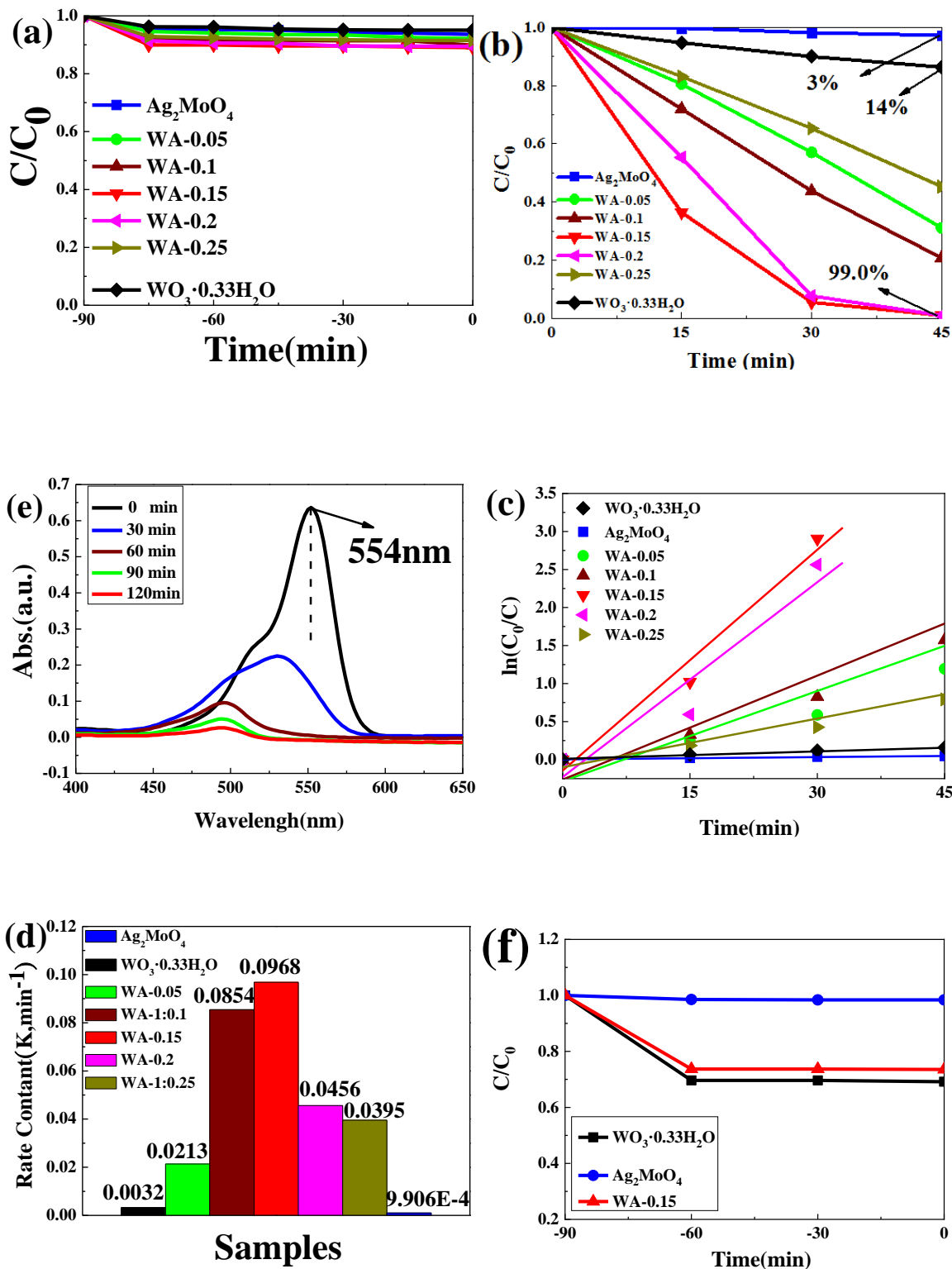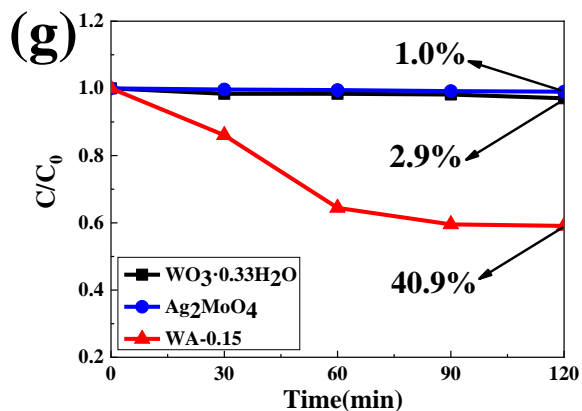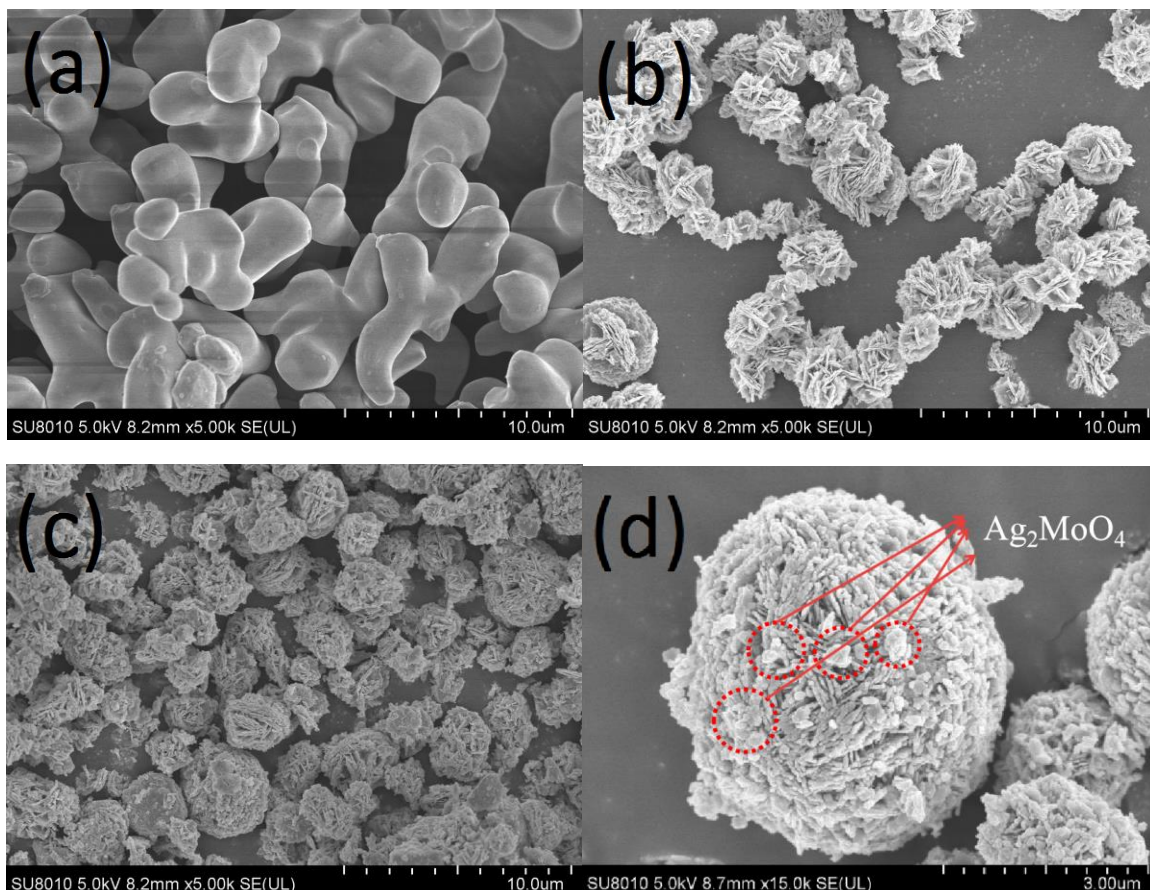
Fig. 2: (a) RhB (100 mL 10 mg/L) adsorption capacity of the samples; (b) The photocatalytic activity for RhB with using different samples; (c) The reaction kinetics of the samples; (d) The reaction rate constants of the samples; (e) UV-vis absorption spectral changes of RhB; (f) LVFX (100 mL 10 mg/L)adsorption capacity of the samples; (g) The Photocatalytic activity of the samples for LVFX
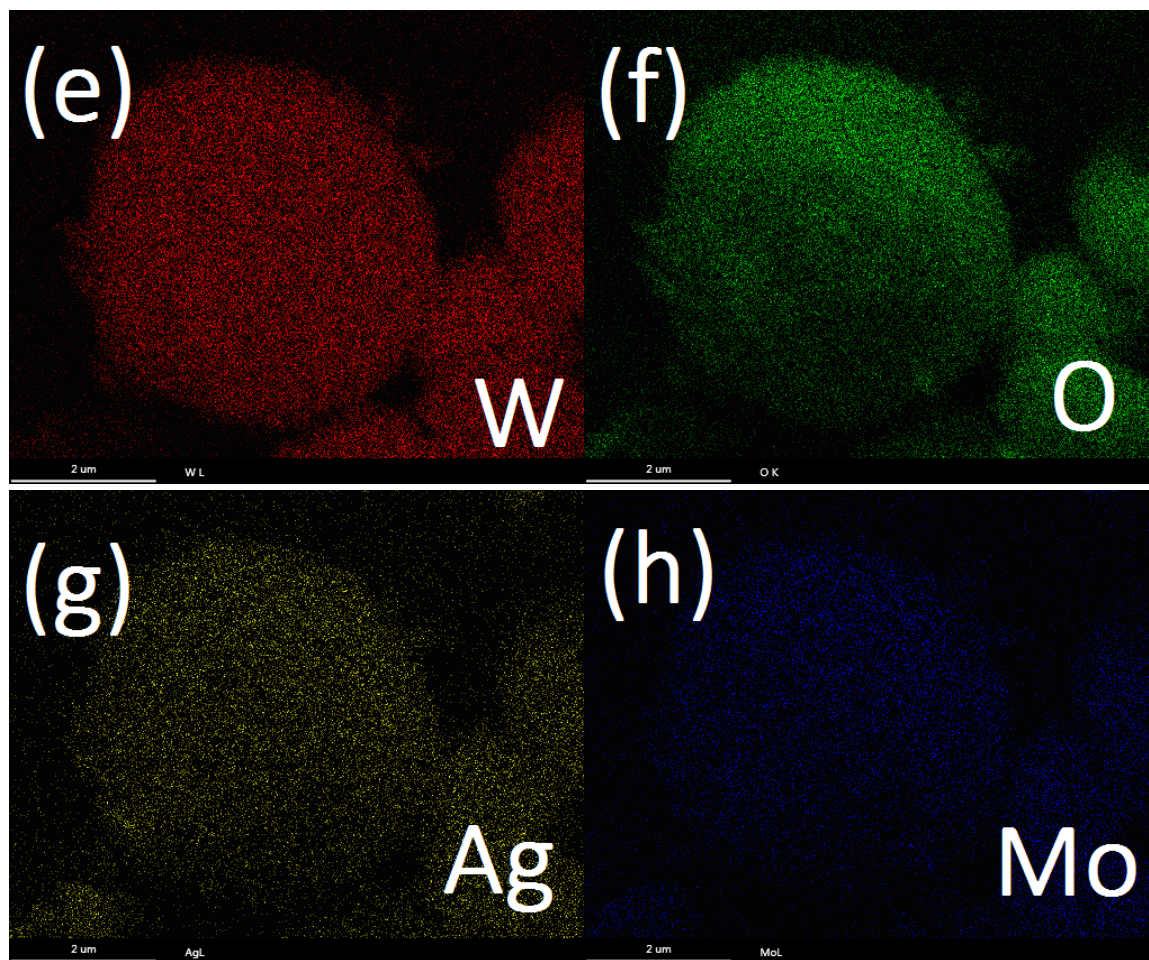
Fig. 3: FE-SEM images of (a) Ag$_2$MoO$_4$, (b) WO$_3$·0.33H$_2$O and (c) WA-0.15 samples; (d) High magnification image of WA-0.15 samples; EDS of WA-0.15 samples: (e) W, (f) O, (g) Ag and (h) Mo.

Generally, Equation (3) can be used to determine the band gap width of semiconductor [27]:

$$\alpha h\nu = A\left(h\nu - E_g\right)^{n/2} \qquad (3)$$

where ν, A, α, E_g and n are light frequency, constant, absorption coefficient, band gap energy and the type of electronic transition of semiconductors, respectively. According to the previous report, n = 1 and 4 is for direct and indirect gap semiconductor, respectively [28]. Moreover, in a direct optical transition process, the square of the absorption coefficient is usually linearly proportional to the energy $\left(h\nu\right)$ of the absorbed edge region [26]. Basing on the intercept of the tangent to the plot of $\left(\alpha h\nu\right)^2$ and $\left(\alpha h\nu\right)^{1/2}$ versus photon energy $\left(h\nu\right)$, the E_g of Ag$_2$MoO$_4$, WO$_3$·0.33H$_2$O and WA-0.15 samples can be respectively calculated as 3.19, 2.54 and 2.38 eV, as shown in Fig. 4(b).
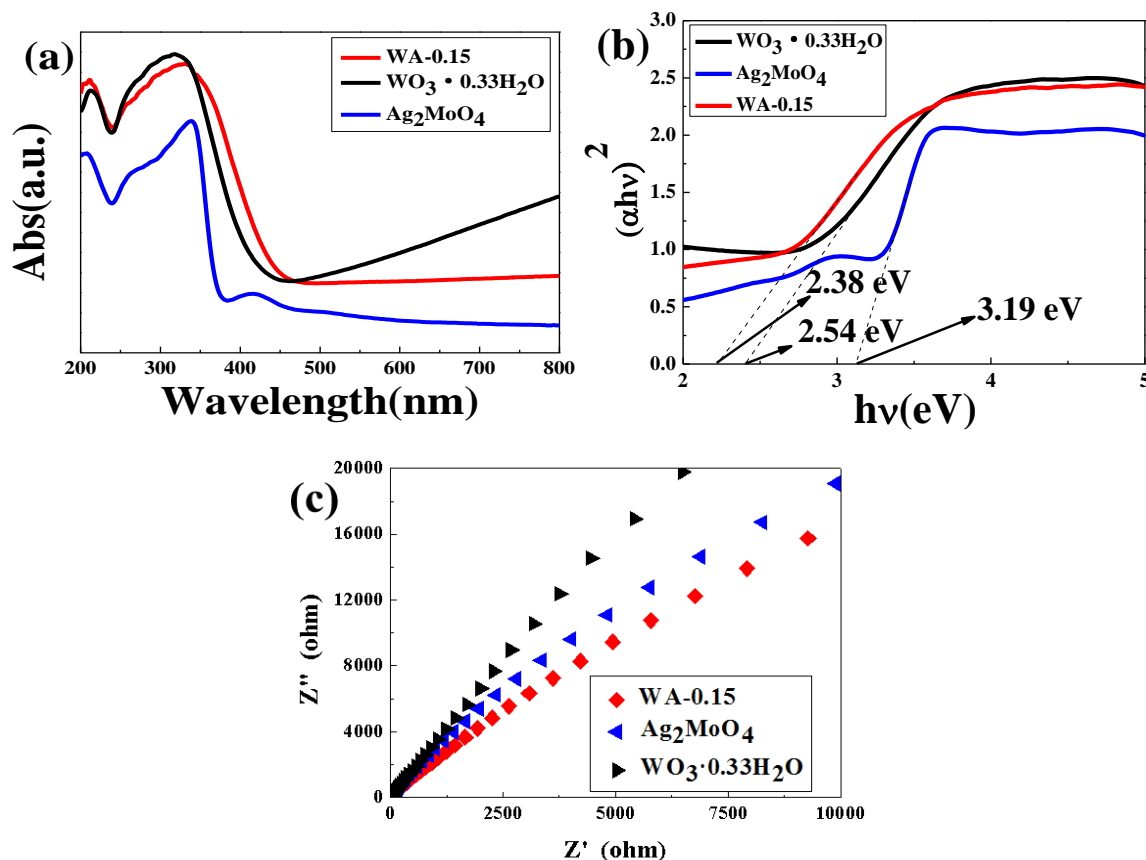
Fig. 4:   (a) UV-vis DRS spectra, (b) plots of $(ahv)^{1/2}$ versus hv and (c) EIS spectra of the samples.

In Fig. 4(c), it can be discovered that the arc radius of WA-0.15 samples is the smallest. This reveals that WA-0.15 samples have the lowest charge transfer resistance and the highest electron-hole separation efficiency. It also indicates that the as-developed WA-0.15 samples can utilize more photons than pure samples under the visible light irradiation.

In Fig. 5 (a), it can be found that there are O, W, Ag and Mo elements in the as-developed WA-0.15 samples. It is worth noting that the characteristic peak of C 1s is also found. This is caused by the carbon species from surface contamination of the samples [26]. In Fig. 5 (b)-(e), it shows the high-resolution XPS spectra of O 1s, W 4f, Ag 3d, and Mo 3d, respectively. In Fig. 5 (b), the characteristic peak of O 1s of WA-0.15 samples is 530.51 eV. This is due to

the oxygen in the crystalline structure of Ag_2MoO_4 and $WO_3 \cdot 0.33H_2O$ [29]. In Fig. 5 (c), the peaks of W $4f_{5/2}$ and W $4f_{7/2}$ of the as-developed WA-0.15 samples can be detected at 35.71 and 35.86 eV, respectively. Compared with $WO_3 \cdot 0.33H_2O$, the peaks shift to the higher energy region. This is leaded by W^{4+}. In Fig. 5 (d) and (e), it shows that the peaks of Ag $3d_{5/2}$, Ag $3d_{3/2}$, Mo $3d_{5/2}$ and Mo $3d_{3/2}$ of the as-developed samples are 367.94, 373.97, 231.92 and 235.10 eV, respectively. Compared with pure Ag_2MoO_4, the peaks of the as-developed composites shift to higher energy region. It is caused by Ag^+ and Mo^{6+} ions. The migration of the peaks indicates that the bonding between $WO_3 \cdot 0.33H_2O$ and Ag_2MoO_4 is chemical rather than physical contact. The electron migration in the as-developed composites is beneficial to reduce the interface energy between these two semiconductors [30].
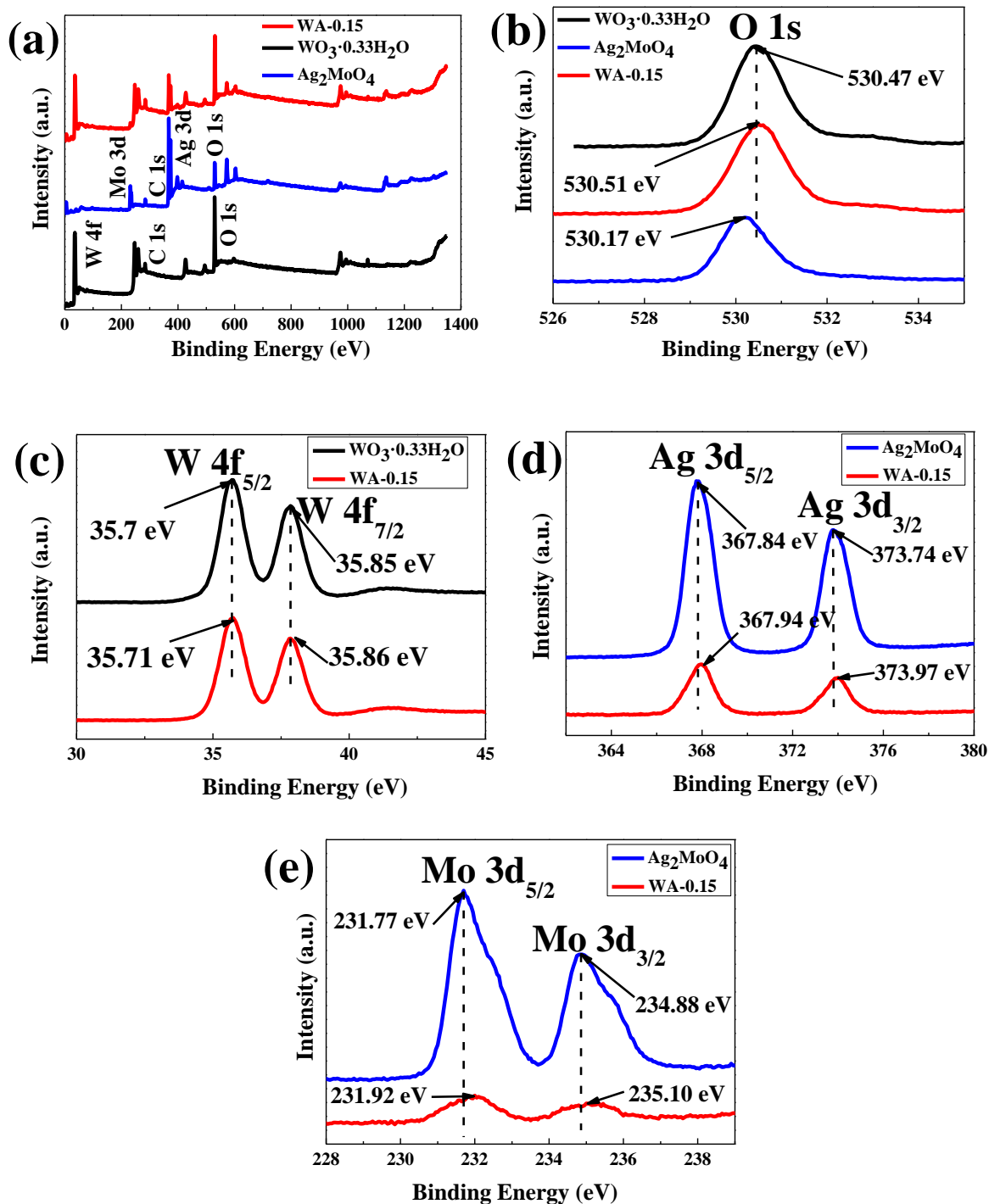
Fig 5: (a) XPS spectra of Ag₂MoO₄, WO₃·0.33H₂O and WA-0.15 samples, (b) O 1s; (c) W 4f of WO₃·0.33H₂O and WA-0.15 samples; (d) Ag 3d and (e) Mo 3d of Ag₂MoO₄ and WA-0.15
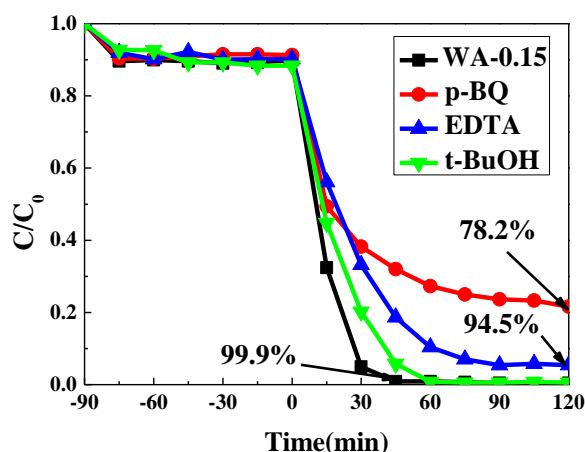
Fig. 6: The effects of different quenchers on the photocatalytic degradation of RhB by using WA-0.15 (In this experiment, 100 mL solution was used as the standard, and the dosage of P-BQ, EDTA and t-BuOH was 0.5, 10 and 10 mmoL in turn.)

In order to analyze the photocatalytic mechanism of the as-developed hybrids for degradation contaminants under the visible light, ethylenediaminetetraacetic acid (EDTA), p-benzoquinone (p-BQ) and tert-butanol (t-BuOH) were used as quenchers for photo-generated holes (h^+) superoxide radicals ($\cdot O_2^-$) and hydroxyl radicals ($\cdot OH$) [31-33], respectively. In this experiment, 100 mL solution was used as the standard, and the dosage of P-BQ, EDTA and t-BuOH was 0.5, 10 and 10 mmoL in turn. It can be discovered in Fig. 6 that the degradation efficiency decreases from 99.9 to 78.2% when p-BQ is used. This reveals that that $\cdot O_2^-$ play a leading role during the degradation reaction. Moreover, it decreases to 94.5% when EDTA is adopted. This means that h^+ play a secondary role during the degradation reaction.

Moreover, in order to further discuss the photocatalytic degradation mechanism of the composites, Equation (4) and (5) are used to calculate the band positions of photocatalyst [5]:

$$E_{CB} = \chi - E_e - 0.5E_g \qquad (4)$$

$$E_{VB} = E_g + E_{CB} \qquad (5)$$

where χ and E_e are the absolute electronegativity of the semiconductor and the energy of free electrons on the hydrogen scale (about 4.5 eV vs. NHE), respectively.

It can be known in Fig. 4 (b) that the E_g of Ag_2MoO_4 and $WO_3 \cdot 0.33H_2O$ are 3.19 and 2.54 eV, respectively. Moreover, the E_{VB} of Ag_2MoO_4 and $WO_3 \cdot 0.33H_2O$ in Fig. 7 are 1.49 and 1.92 eV, respectively. Furthermore, the E_{CB} of Ag_2MoO_4 and $WO_3 \cdot 0.33H_2O$ can be known as -1.70 and -0.62 eV, respectively.
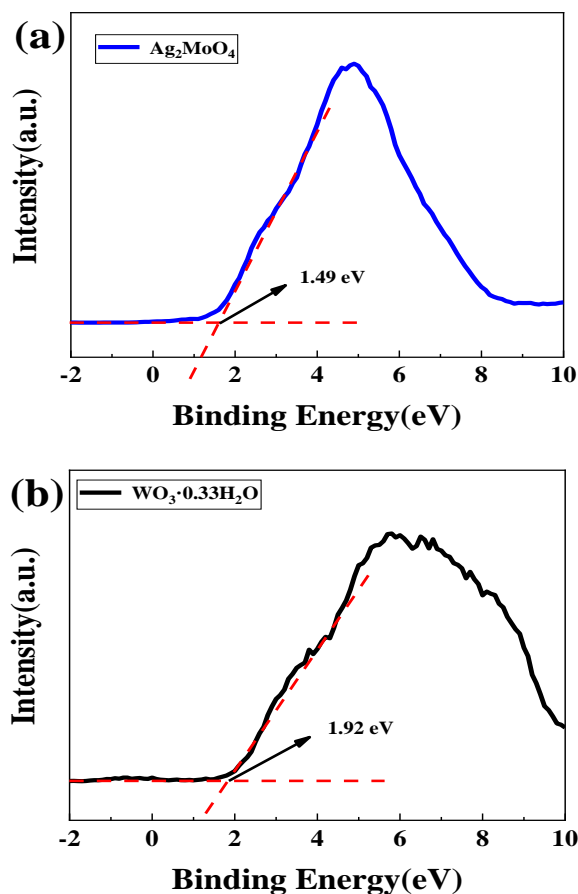

Fig. 7: Valence-band XPS spectra of (a) Ag_2MoO_4 and (b)$WO_3 \cdot 0.33H_2O$.

Under the excitation of visible light, Ag_2MoO_4 and $WO_3 \cdot 0.33H_2O$ absorb photon energy and transfer the electrons of the sample from VB to CB. According to above dates, it can be known that the VB and CB of Ag_2MoO_4 is higher than that of $WO_3 \cdot 0.33H_2O$; therefore the photo-generated electrons of Ag_2MoO_4 can move to CB of $WO_3 \cdot 0.33H_2O$, the photo-generated h^+ of $WO_3 \cdot 0.33H_2O$ can move to VB of Ag_2MoO_4. In the

process of photocatalytic degradation contaminants, the O_2, adsorbed on the surfaces of photocatalyst, reacts with photo-generated electrons to yield $\cdot O_2^-$. In addition, the h^+ react with H_2O to form $\cdot OH$. With the action of two active groups of $\cdot O_2^-$ and $\cdot OH$, RhB and LVFX can be degraded into small non-polluting molecules, such as CO_2 and H_2O [34].

Conclusion

To sum up, in this work, $WO_3 \cdot 0.33H_2O/Ag_2MoO_4$ composite photocatalytic material was prepared by using an *in-situ* growth method. Its microstructure and macroscopic photocatalytic performance were systematically characterized, and the mechanism of its cooperative photocatalytic degradation of organic dye RhB and antibiotic LVFX solution was also explored. The following conclusions were obtained:

(1) XRD test results show that the composite photocatalyst is of high purity, including $WO_3 \cdot 0.33H_2O$ and Ag_2MoO_4 phase, and the diffraction peak of Ag_2MoO_4 increases gradually with the increase of its content in the composite.

(2) The photocatalytic degradation performance test results show that the content of Ag_2MoO_4 in the composite materials significantly affects its photocatalytic performance. With increasing the usage content of Ag_2MoO_4, it shows the tendency of first increasing and then decreasing. When the theoretical molar ratio of $WO_3 \cdot 0.33H_2O$ and $Na_2MoO_4 \cdot 2H_2O$ is 1:0.15, the composite photocatalyst have the optimal photocatalytic activity: that is, 99.0% RhB was degraded within 45min, which is significantly higher than 14% of pure $WO_3 \cdot 0.33H_2O$ and 3% of Ag_2MoO_4. Moreover, LVFX is degraded 40.9% within 120min, which is also higher than 2.9% of pure $WO_3 \cdot 0.33H_2O$ and 1.0% of Ag_2MoO_4.

(3) FE-SEM test results show that the diameter of WA-0.15 was about 4-5 μm, and Ag_2MoO_4 are well distributed on the surface of $WO_3 \cdot 0.33H_2O$ spherical particles.

(4) UV-vis DRS test results show that $WO_3 \cdot 0.33H_2O/Ag_2MoO_4$(WA-0.15) composite has a band gap energy of about 2.38 eV, which is enhanced relative to the light response range and absorption efficiency of Ag_2MoO_4.

(5) EIS test results show that compared with $WO_3 \cdot 0.33H_2O/Ag_2MoO_4$(WA-0.15), the separation of photogenerated electrons and hole pairs is more efficient, and the charge transfer between interfaces is faster.

(6) XPS test results show that the binding between $WO_3 \cdot 0.33H_2O$ and Ag_2MoO_4 is chemical bonding rather than physical contact.

(7) The test results of active species show that: $\cdot O_2^-$ and h^+ respectively play a leading and the secondary role during the photocatalytic degradation pollutions.

This technology provides a good guide to prepare visible-light-driven photocatalyst and a success example for treatment of dyes and antibiotics contaminants in water with using solar energy.

Acknowledgments

References

1. H. L. Jiang, X. Q. Li, L. Tian, T. Wang, Q. Wang, P. P. Niu, P. H. Chen and X. B. Luo. Defluoridation investigation of yttrium by laminated Y-Zr-Al tri-metal nanocomposite and analysis of the fluoride sorption mechanism. *Sci. Total Environ.*, **648**, 1342 (2019).

2. C. Chen, W. H. Ma and J. Zhao. Semiconductor-mediated photodegradation of pollutants under visible-light irradiation. *Chem. Soc. Rev.*, **39**, 4206 (2010).

3. Y. J. Wang, X. F. Wu, Z. H. Zhao, H. Li, C. X. Zhang, J. Z. Su, J. R. Zhang, Z. L. Cao, Y. W. Wang, K. Y. Wang and J. C. Pan. Hydrothermal synthesis of Zn_2SnO_4/few-layer boron nitride nanosheets hybrids as a visible-light-driven photocatalyst. *J. Wuhan Univ. Technol.-Mat. Sci. Edit.*, **34**, 563 (2019).

4. S. C. Zhang, Z. F. Liu, M. N. Ruan, Z. G. Guo, L. E, W. Zhao, D. Dan, X. F. Wu and D. M. Chen. Enhanced piezoelectric-effect-assisted photoelectrochemical performance in ZnO modified with dual cocatalysts. *Appl. Catal. B-Environ.*, 262, 118279 (2020).

5. N. C. Zheng, T. Ouyang, Y. B. Chen, Z. D. Wang, Y. Chen and Z. Q. Liu. Ultrathin CdS shell sensitized hollow S-doped CeO_2 spheres for

efficient visible-light photocatalysis. *Catal. Sci. Technol.*, **9**, 1357 (2019).

6. X. F. Wu, H. Li, J. Z. Su, J. R. Zhang, Y. M. Feng, Y. N. Jia, L. S. Sun, W. G. Zhang, M. Zhang and C. Y. Zhang. Full spectrum responsive In₂.₇₇S₄/WS₂ p-n heterojunction as an efficient photocatalyst for Cr(VI) reduction and tetracycline oxidation. *Appl. Surf. Sci.*, **473**, 992 (2019).

7. N. Kulik, Y. Panova and M. Trapido. The fenton chemistry and its combination with coagulation for treatment of dye solutions. *Sep. Sci. Technol.*, **42**, 1521 (2007).

8. K. Ikehata, M. G. El-Din and S. A. Snyder. Ozonation and advanced oxidation treatment of emerging organic pollutants in water and wastewater. *Ozone: Science and Engineering*, **30**, 21 (2008).

9. D. P. Singh, B. Sirota, S. Talpatra, P. Kohli, C. Rebholz and S. M. Aouadi. Broom-like and flower-like heterostructures of silver molybdate through pH controlled self assembly. *J. Nanopart. Res.*, **14**, 781 (2012).

10. S. K. Gupta, P. S. Ghosh, K. Sudarshan, R. Gupta, P. K. Pujari and R. M. Kadam. Multifunctional pure and Eu(3+) doped β-Ag₂MoO₄: photoluminescence, energy transfer dynamics and defect induced properties. *Dalton Trans.*, **44**, 19097 (2015).

11. Y. Y. Bai, F. R. Wang and J. K. Liu. A new complementary catalyst and catalytic mechanism: Ag₂MoO₄/Ag/AgBr/GO heterostructure. *Ind. Eng. Chem. Res.*, **55**, 9873 (2016).

12. Z. F. Wang, D. Q. Chu, L. P. Wang, W. H. Hua, X. Y. Chen and H. F. Yang. EDTA-assisted synthesis of camellia-like WO₃·0.33H₂O architectures with enhanced visible-light-driven photocatalytic activity. *Catal. Commun.*, **88**, 1 (2017).

13. C. Santato, M. Odziemkowski, M. Ulmann and J. Augustynski. Crystallographically oriented mesoporous WO₃ films: Synthesis, characterization, and applications. *J. Am. Chem. Soc.*, **123**, 10639 (2001).

14. D. H. Kim. Effects of phase and morphology on the electrochromic performance of tungsten oxide nano-urchins. *Sol. Energy Mater. Sol. Cells*, **107**, 81 (2012).

15. Y. F. Guo, X. Quan, N. Lu, H. M. Zhao and S. Chen. High photocatalytic capability of self-assembled nanoporous WO₃ with preferential orientation of (002) planes. *Environ. Sci. Technol.*, **41**, 4422 (2007).

16. X. F. Lu, X. C. Liu, W. J. Zhang, C. Wang and Y. Wei. Large-scale synthesis of tungsten oxide nanofibers by electrospinning. *J. Colloid Interface Sci.*, **298**, 996 (2006).

17. S. Y. An, S. H. Park, Ko and S. H. Fabrication of WO₃ nanotube sensors and their gas sensing properties. *Ceram. Int.*, **40**, 1423 (2014).

18. H. Q. Ren, X. F. Gou and Q. Yang. Ultrathin Ag nanoparticles anchored on urchin-like WO₃·0.33H₂O for enhanced photocatalytic performance. *RSC Adv.*, **7**, 12085 (2017).

19. W. Wei, J. Xie, X. Lü, Z. X. Yan, S. C. Meng and H. L. Cui. CTAB-assisted synthesis and characterization of Bi₂WO₆ photocatalysts grown from WO₃·0.33H₂O nanoplate precursors. *Monatshefte fuer Chemie*, **145**, https://doi.org/10.1007/s00706-013-0994-7 (2014).

20. X. Y. He, C. G. Hu, Y. Xi, K. Y. Zhang and H. Hua. Three-dimensional Ag₂O/WO₃·0.33H₂O heterostructures for improving photocatalytic activity. *Mater. Res. Bull.*, **50**, 91(2014).

21. Z. W. Liu, P. Li, Y. Dong, Q. Wan, F. Q. Zhai, A. A. Volinsky and X. H. Qu. Facile preparation of hexagonal WO₃·0.33H₂O/C nanostructures and its electrochemical properties for lithium-ion batteries. *Appl. Surf. Sci.*, **394**, 70 (2017).

22. Y. S. Li, Z. L. Tang, J. Y. Zhang and Z. T. Zhang. Fabrication of vertical orthorhombic/hexagonal tungsten oxide phase junction with high photocatalytic performance. *Appl. Catal. B-Environ.*, **207**, 207 (2017).

23. J. Y. Zhang, Y. Lu, J. K. Liu and H. Jiang. Mosaic structure effect and superior catalytic performance of AgBr/Ag₂MoO₄ composite materials. *RSC Adv.*, **6**, 94771 (2016).

24. Y. M. Feng, Z. Q. Wang, Y. F. Yang, X. F. Wu, X. D. Gong, Y. J. Liu, Y. F. Li, Z. L. Cao, C. Wang and X. Tong. Chemical-bonds-conjugated Ag₂SO₃/NaNbO₃ hybrids as effcient photocatalysts: In-situ fabrication, characterization and degradation of rhodamine B and methyl orange. *Nano*, **13**, https://doi.org/10.1142/S1793292018500765 (2018).

25. X. F. Wu, H. Li, J. C. Pan, Y. J. Wang, C. X. Zhang, J. Z. Su, J. R. Zhang, Y. Zhang, W. G. Zhang, L. S. Sun and X. G. Sun. Designing visible-light-driven direct Z-scheme Ag₂WO₄/WS₂ heterojunction to enhance photocatalytic activity. *J. Mater. Sci.-Mater. Electron.*, **29**, 14874 (2018).

26. J. L. Zhang and Z. Ma. Novel b-Ag₂MoO₄/g-C₃N₄ heterojunction catalysts with

highly enhanced visible-light-driven photocatalytic activity. *RSC Adv.*, **7**, 2163 (2017).

27. X. F. Wu, H. Li, L. S. Sun, J. Z. Su, J. R. Zhang, W. G. Zhang, M. Zhang, G. W. Sun, L. Zhan and M. Zhang. One-step hydrothermal synthesis of visible-light-driven $In_{2.77}S_4/SrCO_3$ heterojunction with efficient photocatalytic activity for degradation of methyl orange and tetracycline. *Appl. Phys. A-Mater. Sci. Process.*, **124**, https://doi.org/10.1007/s00339-018-2012-8 (2018).

28. X. F. Wu, Y. Sun, H. Li, Y. J. Wang, C. X. Zhang, J. R. Zhang, J. Z. Su, Y. W. Wang, Y. Zhang, C. Wang and M. Zhang. In-situ synthesis of novel p-n heterojunction of Ag_2CrO_4-$Bi_2Sn_2O_7$ hybrids for visible-light-driven photocatalysis. *J. Alloy. Compd.*, **740**, 1197 (2018).

29. S. Xu, D. F. Fu, K. Song, L. Wang, Z. B. Yang, W. Y. Yang and H. L. Hou. One-dimensional $WO_3/BiVO_4$ heterojunction photoanodes for efficient photoelectrochemical water splitting. *Chem. Eng. J.*, **349**, 368 (2018).

30. J. X. Yu, Q. Y. Nong, X. L. Jiang, X. Z. Liu, Y. Wu and Y. M. He. Novel $Fe_2(MoO_4)_3/g$-C_3N_4 heterojunction for efficient contaminant removal and hydrogen production under visible light irradiation. *Sol. Energy*, **139**, 355 (2016).

31. Z. H. Xu, M. Quintanilla, F. Vetrone, A. Govorov, M. Chaker and D. L. Ma. Harvesting lost photons: Plasmon and upconversion enhanced broadband photocatalytic activity in core@shell microspheres based on lanthanide-doped $NaYF_4$, TiO_2, and Au. *Adv. Funct. Mater.*, **25**, 2950 (2015).

32. S. P. Ding, X. F. Liu, Y. Q. Shi, Y. Liu, T. Z. Zhou, Z. P. Guo and J. C. Hu. Generalized synthesis of ternary sulfide hollow structures with enhanced photocatalytic performance for degradation and hydrogen evolutio. *ACS Appl. Mater. Interfaces,*, **10**, 17911 (2018).

33. G. Gogoi, S. Keene, A. S. Patra, T. K. Sahu, S. Ardo and M. Qureshi. A novel hybrid of g-C_3N_4 and MoS_2 integrated onto $Cd_{0.5}Zn_{0.5}S$: Rational design with efficient charge transfer for enhanced photocatalytic activity. *ACS Sustain. Chem. Eng.*, **6**, 6718 (2018).

34. J. Wang, G. K. Zhang, J. Li and K. Wang. Novel 3D flower-like $BiOBr/Bi_2SiO_5$ p-n heterostructured nanocomposite for degradation of tetracycline: enhanced visible light photocatalytic activity and mechanism. *ACS Sustain. Chem. Eng.*, **6**, 14221 (2018).